Supporting Information:

Precisely calibrated and spatially informed illumination for conventional fluorescence and improved PALM imaging applications

Angel Mancebo[1], Luke DeMars[1], Christopher T. Ertsgaard[1] and Elias M. Puchner[1#]

[1]School of Physics and Astronomy
University of Minnesota, Twin Cities
Physics and Nanotechnology (PAN)
115 Union Street SE, Minneapolis, MN 55455

corresponding author, e-mail: epuchner@umn.edu

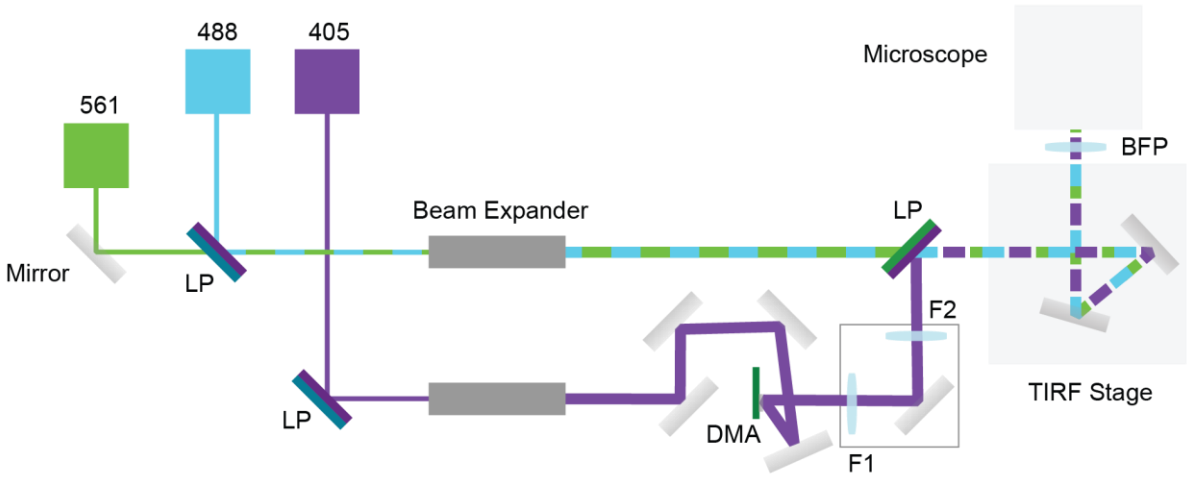

Figure S1: Optical layout of the conventional and DMA excitation path. In the conventional excitation path, the 561 nm and 488 nm lasers are combined with a low pass filter (LP), expanded by an 8x and 2x beam expander, and their diameters are restricted with an iris to block the low intensity portion of the gaussian profile. The 405 nm laser can be decoupled from the conventional excitation path by moving the low pass filter (LP) to the lower excitation path, where the laser gets expanded by a separate 8x and 2x beam expander and restricted by an iris. The 405 nm laser gets reflected by mirrors onto the DMA at an angle of incidence of 24° to the DMA surface normal. This angle is the blaze angle of the DMA and is required to maximize diffraction efficiency and for the reflection to be parallel to the DMA surface normal. The diffraction of the DMA causes diverging orders which are captured by a 4F near the source to maximize power transmission and to form the DMA image at the focal point of the microscope objective. F1 (diameter: 1 in, focal length: 50.2 mm) is mounted at the focal length of 50.2 mm away from the DMA, F2 (diameter: 2 in, focal length: 150 mm) is mounted at an optical path length of 200.2 mm away from F1 (sum of focal lengths). The portion of the 405 nm laser that is reflected from the DMA then gets combined with the 488 nm and 561 nm laser with a long pass filter (LP) and reflected through mirrors on a motorized TIRFF stage through the back-focal plane lens (BFP, diameter 2 in, focal length: 400 mm). BFP is mounted at an optical path distance of 550 mm away from F2 and focuses the expanded and spatially patterned lasers in the back focal plane of the objective, which superimposes the captured orders in the sample plane.

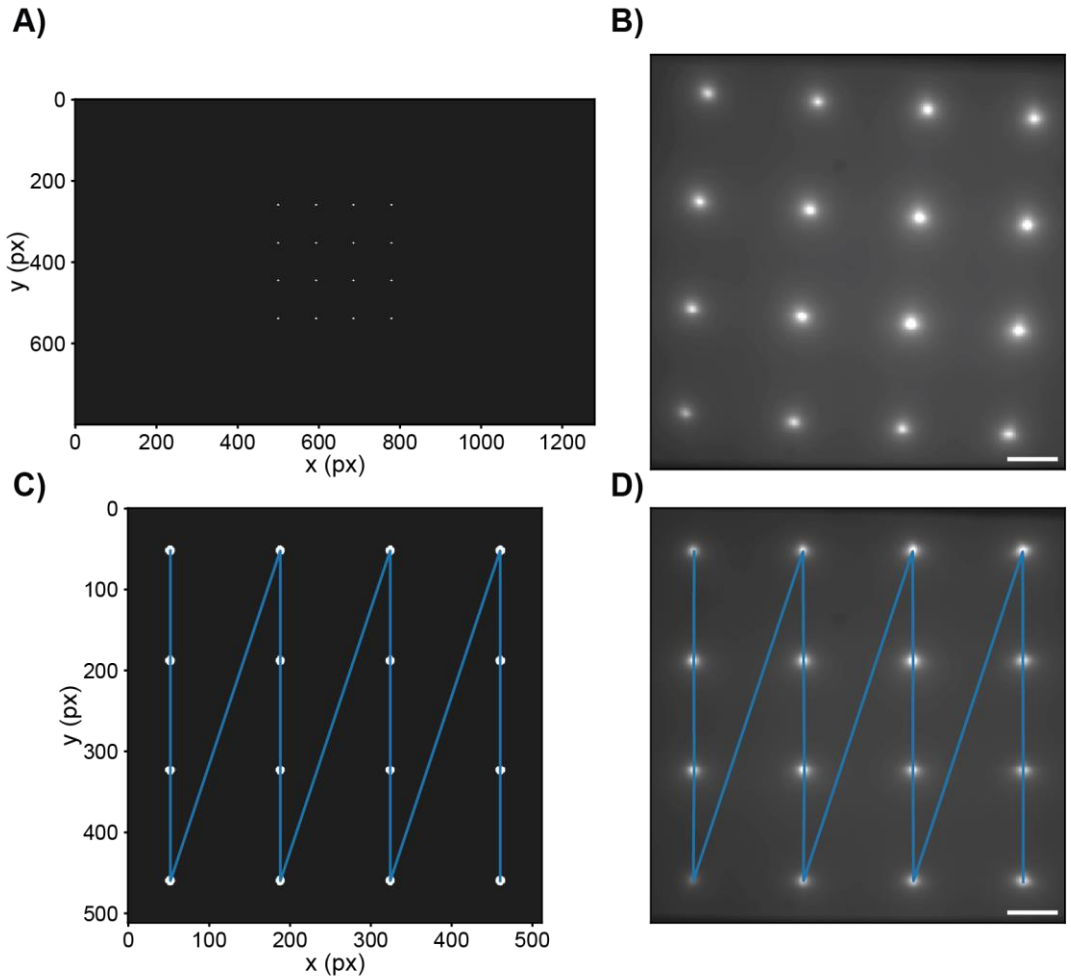

Figure S2: C**alibration approach to precisely match the DMA and camera coordinate system.** (A) Pattern sent to the DMA for calibration with white pixels reflecting the incident 405 nm laser. (B) Camera image of the fluorescein emission from the DMA pattern in the sample plane. Note the distortion of the pattern compared to (A). (C) Calibration validation pattern in the coordinate system of the camera. (D) The calibration validation pattern is warped with the 3rd-order inverse transformation (that maps (B) to (A)) and sent back to the DMA. The resulting fluorescein emission recorded with the camera matches the calibration validation pattern in C) and proofs accurate calibration. Scale bars are 5µm.

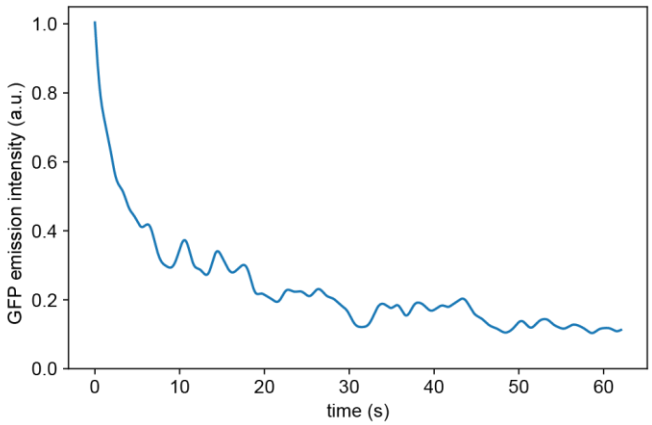

Figure S3: FRAP bleaching curve. Mean GFP emission intensity (488 nm excitation) from the region selected for FRAP during bleaching (see Fig. 2).

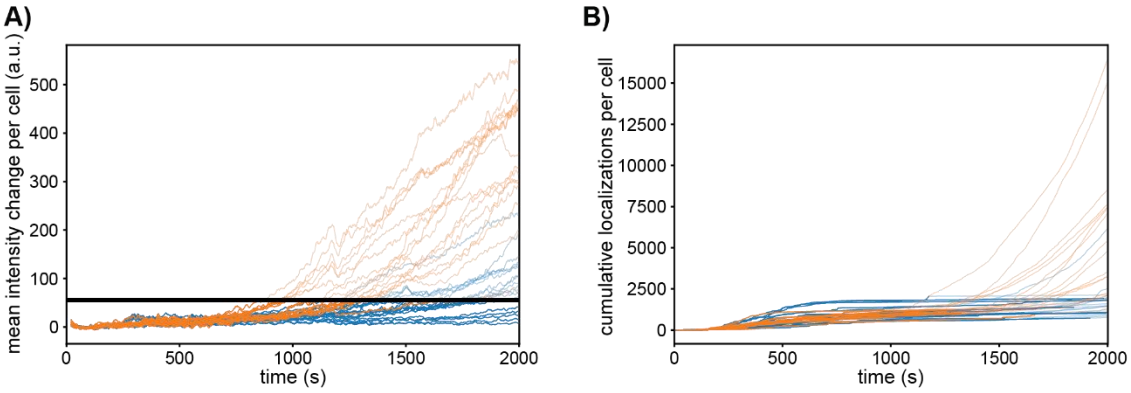

Figure S4: Determination of cutoff intensity and times for single-molecule localizations. (A) Mean intensity change traces (561 nm excitation) and (B) cumulative count traces for individual fully (orange) and partially photoactivated (blue) cells. The cutoff intensity used for determining when to stop considering localizations is shown in black (transition to unhealthy state). Traces are plotted semi-transparent after reaching the mean intensity threshold.

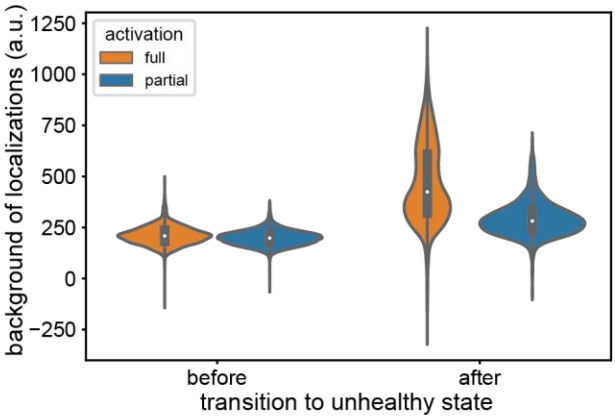

Figure S5: Comparison of single-molecule background intensities. Violin plot of single-molecule background intensity before and after respective cutoff time for each cell separated by fully and partially photoactivated (orange and blue, respectively). The fully illuminated cells develop a bimodal distribution with broad peaks, the higher background peak corresponding to false localizations, while the partially illuminated cells only develop a broadening and a slight increase in the intensity of the background peak. The inside of each violin contains a boxplot. Boxes extend from the 25th to 75th percentiles (interquartile range, IQR). Medians are shown as white circles. Whiskers extend to the farthest data point within 1.5 IQR below and above the 25th and 75th percentiles, respectively. Individual data and outliers are not shown. 0.2% of fits did not converge properly causing the violins and whiskers to extend below zero.

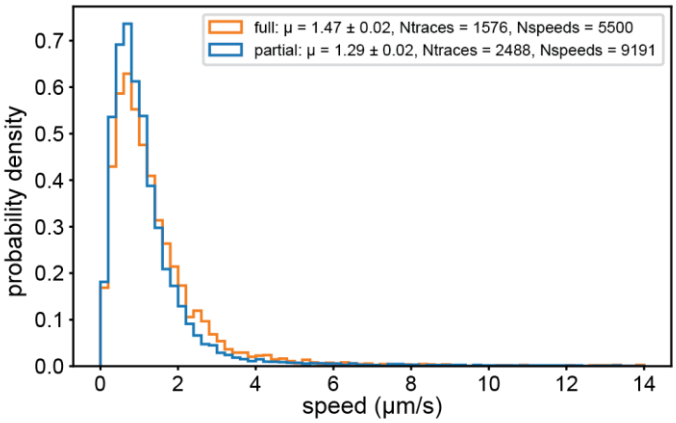

Figure S6: Probability density of molecule speeds computed from frame-to-frame step sizes divided by the exposure time. Traces recorded after the transition of a cell to the unhealthy state were excluded. There is no significant difference in molecule speed distribution between fully and partially photoactivated cells. Mean ± std from bootstrapping (n=10,000).

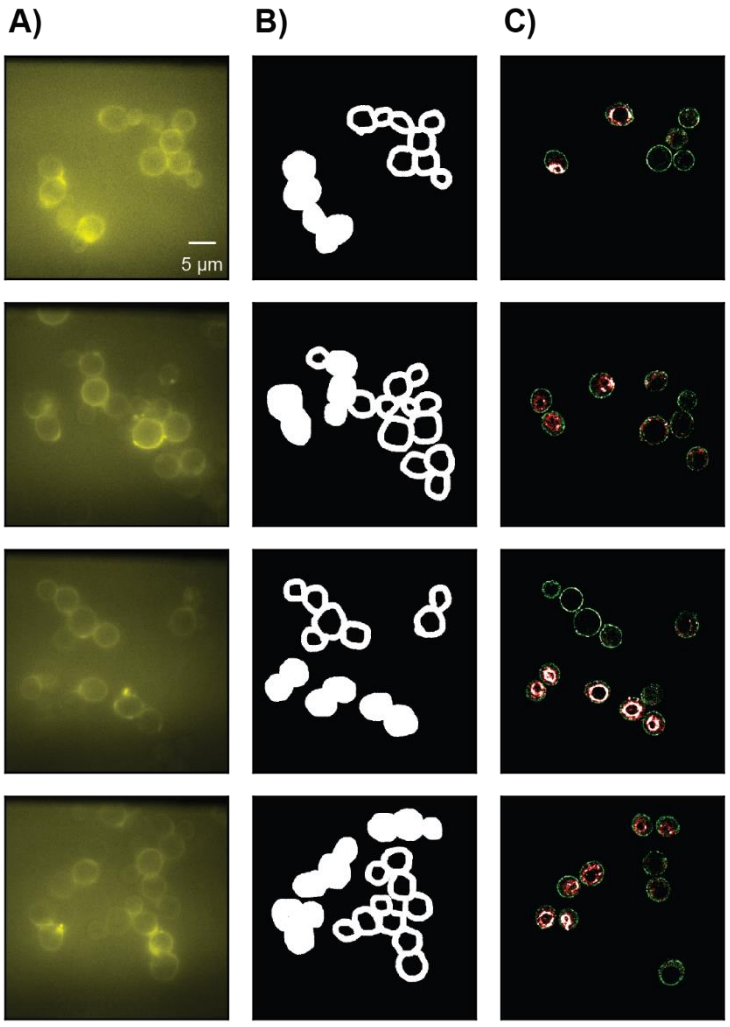

Figure S7: Demonstration of informed photoactivation across the full field of view for all cells used in the analysis. (A) CF488M emission from 488 nm excitation. (B) Photoactivation masks for cells in (A). (C) Rendered super-resolution images of mEos2 localizations while cells are healthy (green) and after the transition to the unhealthy state. Only cells that were not too out of focus to show single-molecules at the PM and did not drift during acquisition in the healthy state were selected for intensity cutoff time analysis, and hence shown in the rendering. Scale bar is 5 µm and the scale is the same for all figures.

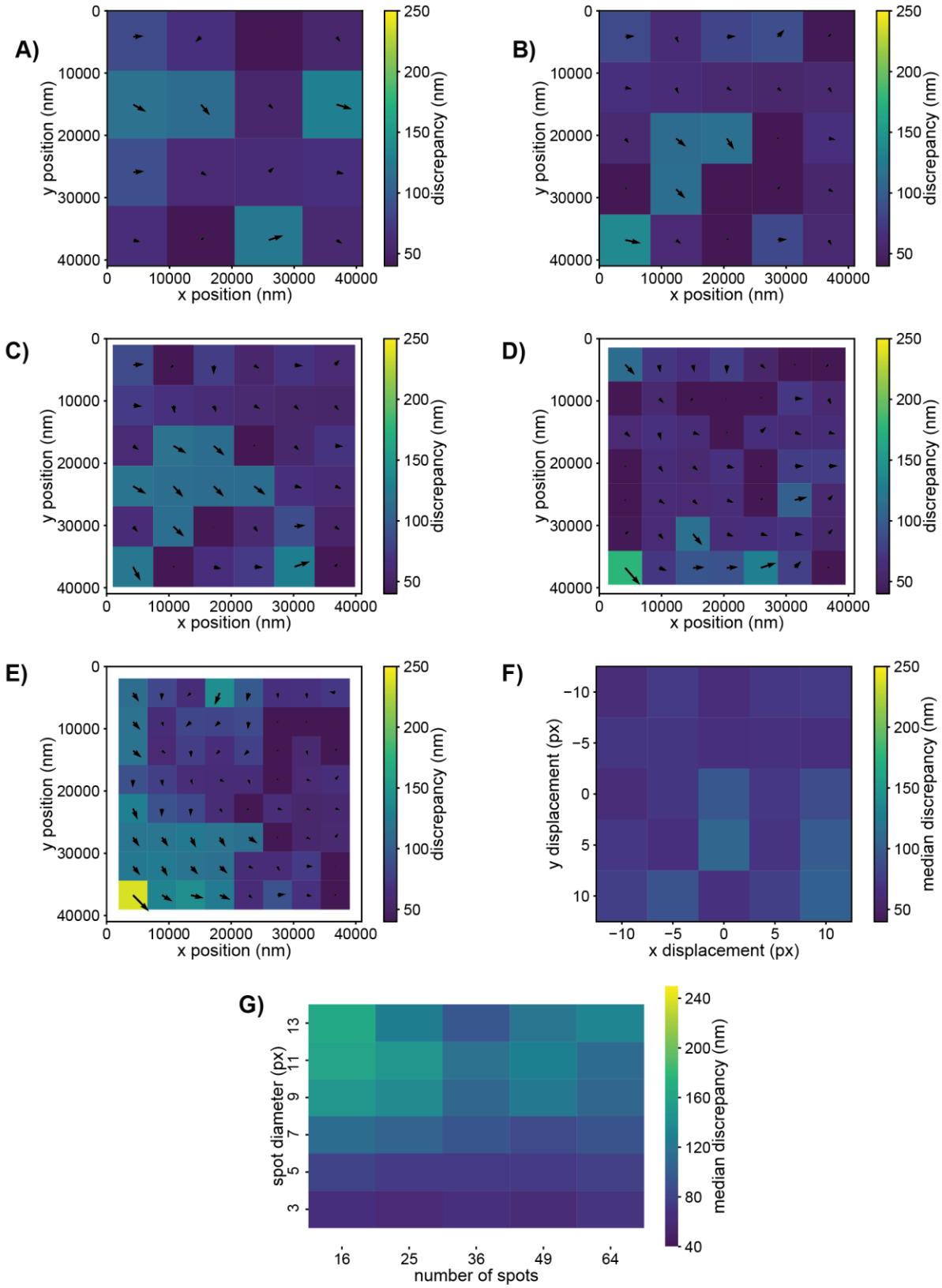
A)
B)
C)
D)
E)
F)
G)
y position (nm)
x position (nm)
discrepancy (nm)
y displacement (px)
x displacement (px)
median discrepancy (nm)
spot diameter (px)
number of spots

Figure S8: Calibration procedure characterization. The calibration procedure was performed as described in the materials and methods and as shown in Fig. S2. We systematically varied the spot diameter, the number of spots, and the central position of the calibration pattern to characterize the procedure. The spot diameter was varied while keeping the spot position constant. Smaller spot diameters yielded lower overall emission intensity due to delivering less of the laser's total power. The number of spots was varied by keeping the covered area constant and varying the density of spots. Larger numbers of spots generally yielded higher intensity signals due to the increased density of spots. The laser intensity was kept constant for each spot diameter with a reduction in intensity in cases when the signal saturated the camera. The size of the verification spots was scaled to approximate the size of the original calibration spots. (A-E) The calibration was performed using a pattern with spots arranged in 4×4, 5×5, 6×6, 7×7, and 8×8, respectively, with a spot diameter of 3 pixels. Color represents magnitude of the discrepancy. The arrows represent the direction and relative magnitude of the discrepancy of measured from projected spot positions. The arrow tails begin at the projected spot positions. (F) Median discrepancy of spots for an 8×8 calibration pattern shifted from its central position by 5 pixels at a time in each direction with a fixed spot diameter of 3 pixels. (G) Median discrepancy of spots for different spot diameters and numbers of spots.